



Seasonal Antarctic pressure variability during the twentieth century from spatially complete reconstructions and CAM5 simulations

Ryan L. Fogt¹ · David P. Schneider² · Chad A. Goergens¹ · Julie M. Jones³ · Logan N. Clark¹ · Michael J. Garberoglio¹

Received: 12 April 2018 / Accepted: 7 February 2019 / Published online: 22 February 2019
© Springer-Verlag GmbH Germany, part of Springer Nature 2019

Abstract

As most permanent observations in Antarctica started in the 1950s, understanding Antarctic climate variations throughout the twentieth century remains a challenge. To address this issue, the non-summer multi-decadal variability in pressure reconstructions poleward of 60°S is evaluated and assessed in conjunction with climate model simulations throughout the twentieth and early twenty-first centuries to understand historical atmospheric circulation variability over Antarctica. Austral autumn and winter seasons show broadly similar patterns, with negative anomalies in the early twentieth century (1905–1934), positive pressure anomalies in the middle twentieth century (1950–1980), and negative pressure anomalies in the most recent period (1984–2013), consistent with concurrent trends in the SAM index. In autumn, the anomalies are significant in the context of estimates of interannual variability and reconstruction uncertainty across most of the Antarctic continent, and the reconstructed patterns agree best with model-generated patterns when the simulation includes the forced response to tropical sea surface temperatures and external radiative forcing. In winter and spring, the reconstructed anomalies are less significant and are consistent with internal atmospheric variability alone. The specific role of tropical SST variability on pressure trends in these seasons is difficult to assess due to low reconstruction skill in the region of strongest tropical teleconnections, the large internal atmospheric variability, and uncertainty in the SST patterns themselves. Indirect estimates of pressure variability, whether through sea ice reconstructions, proxy records, or improved models and data assimilation schemes, will help to further constrain the magnitude of internal variability relative to the forced responses expected from SST trends and external radiative forcing.

1 Introduction

Compared to many other regions, changes in the Antarctic climate are more difficult to attribute to human activity, primarily because of the large interannual variability and short nature of Antarctic records (Jones et al. 2016). Nonetheless, during austral summer, many studies have noted a significant

impact of ozone depletion on the Antarctic climate since 1980, manifested as decreases in summer pressure over and around the Antarctic continent and the associated positive trend in the Southern Annular Mode index (Thompson and Solomon 2002; Marshall 2003; Miller et al. 2006; Fogt et al. 2009, 2017a; Polvani et al. 2011; England et al. 2016; Jones et al. 2016). In the other seasons, ozone depletion and increasing greenhouse gas concentrations appear to play a more minor role in Antarctic climate variability and change compared to the large natural variability, including variability from tropical sea surface temperatures (SSTs; Ding et al. 2011; Schneider et al. 2012; Ding and Steig 2013; Fogt and Zbacnik 2014; Clem and Fogt 2015; Fogt and Wovrosh 2015; Meehl et al. 2016; Jones et al. 2016; Purich et al. 2016).

To help assess the natural Antarctic climate variability, multiple new datasets have been developed to extend the limited observational record either spatially or temporally throughout the twentieth century. These include several temperature reconstructions back to 1957 that documented the

Electronic supplementary material The online version of this article (<https://doi.org/10.1007/s00382-019-04674-8>) contains supplementary material, which is available to authorized users.

✉ Ryan L. Fogt
fogtr@ohio.edu

¹ Department of Geography and Scalia Laboratory for Atmospheric Analysis, Ohio University, 122 Clippinger Laboratories, Athens, OH 45701, USA

² National Center for Atmospheric Research, Boulder, CO, USA

³ Department of Geography, University of Sheffield, Sheffield, UK

warming of both West Antarctica and the Antarctic Peninsula since the International Geophysical Year (1957–1958; Monaghan et al. 2008; Steig et al. 2009; O'Donnell et al. 2011; Nicolas and Bromwich 2014), although due to the large natural variability, temperature trends on the Antarctic Peninsula have weakened since 2000 (Turner et al. 2016). Most recently, seasonal pressure reconstructions aimed at understanding the atmospheric circulation on and around the Antarctic continent since 1905 have been developed and evaluated for both individual stations (Fogt et al. 2016a, b) and spatially poleward of 60°S for austral summer (Fogt et al. 2017a). These pressure reconstructions show the dominance of stratospheric ozone depletion in the summer season on the recent negative pressure trends, but with important contributions from tropical SSTs on these negative trends as well as periods of previous summer pressure variability (Fogt et al. 2017a), including the race to the South Pole during the austral summer of 1911–1912 (Fogt et al. 2017b).

The goal of this work is to extend the seasonal summer spatial pressure reconstructions to the other seasons, evaluate their performance, and document non-summer Antarctic pressure changes throughout the entire twentieth century. To help determine the role of various mechanisms influencing the Antarctic atmospheric circulation, we also employ century-length simulations from a non-coupled climate model with prescribed tropical SSTs and different configurations of radiative forcings. Given that most studies have documented the importance of natural variability stemming from the tropics outside of austral summer, the combination of spatially complete seasonal pressure reconstructions and climate models with prescribed tropical SSTs is ideal to advance the understanding of historic Antarctic pressure variability. This is especially important since the consistency between the various century-length reanalysis products is considerably lower before 1957 due to the sparse and sporadic nature of early Antarctic meteorological observations (Schneider and Fogt 2018).

2 Data

2.1 Antarctic pressure data and station reconstructions

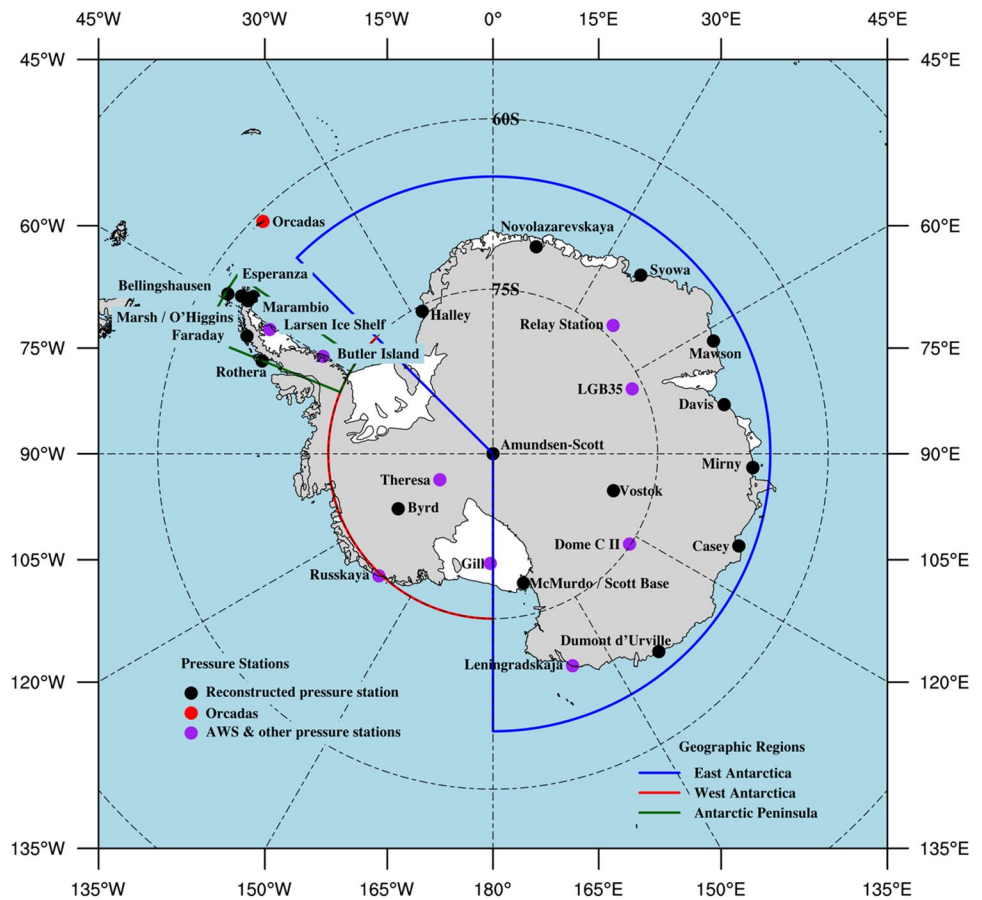
Monthly mean pressure records from staffed research stations and automatic weather stations are obtained from the Reference Antarctic Data for Environmental Research (READER; <http://www.antarctica.ac.uk/met/READER>) archive (Turner et al. 2004) (see Fig. 1 for locations). The pressure observations were extended throughout the twentieth century at each station except Orcadas (Zazulie et al. 2010) from reconstructions discussed in Fogt et al. (2016a, b). As noted by Fogt et al. (2016a), the performance of the

pressure reconstructions conducted at each station varies seasonally. Outside of austral summer, the pressure reconstructions at each Antarctic station that were based on a blend of primarily Southern Hemisphere (SH) mid-latitude pressure observations and gridded climate data at select ocean grid points aligned better with the Antarctic observations after 1957 than those based solely on SH mid-latitude pressure data. As such, we employ here the former station pressure reconstructions (termed ‘pseudo-reconstructions’ by Fogt et al. 2016a) for the non-summer spatial Antarctic pressure reconstruction, and only compare to the spatial reconstruction for summer discussed in Fogt et al. (2017a). As in this work, we make use of the European Centre for Medium Range Weather Forecasts (ECMWF) Interim reanalysis (ERA-Interim) to generate and evaluate the spatial pressure reconstruction, and convert all data to pressure anomalies by removing the 1981–2010 climatological mean from all gridpoints. In all cases, a traditional definition of the austral seasons is used: summer, December–February (DJF); autumn, March–May (MAM); winter, June–August (JJA); and spring, September–November (SON).

2.2 Antarctic spatial pressure reconstruction

The method to create the spatial reconstruction is the same as in Fogt et al. (2017a), and is only briefly repeated here. The domain is a polar stereographic 80 km × 80 km Cartesian grid centered over the South Pole, and extending equatorward to 60°S. We employ a kriging method to interpolate the seasonal station pressure reconstructions from Fogt et al. (2016a, b), based on weights generated from ERA-Int reanalysis data during the model calibration period of 1979–2013 along with the 19 stations in Fig. 1; the spatial reconstruction is not based on any direct observations, only the station pressure reconstructions from Fogt et al. (2016a, b). As in Nicolas and Bromwich (2014), the kriging weights are optimized to avoid over-fitting the model and are based on the covariances between the 19 stations used in the interpolation and the relationship each of these stations have with each of the grid points on the Cartesian grid. Once the weights are determined, they are used in connection with the anomalies from the individual station pressure reconstructions (Fogt et al. 2016a, b) and the Orcadas observational record to produce a spatially complete surface pressure anomaly reconstruction over the Antarctic continent back to 1905; the climatological mean from ERA-Int can further be added at each grid point to make the reconstruction in terms of surface pressure. We also employ the same validation approach of Fogt et al. (2017a) by determining the kriging weights separately for the periods 1979–1996 and 1997–2013. These kriging weights are then used to produce an independent

Fig. 1 Map of the reconstructed station pressure locations (black), observations from Orcadas (red), and AWS locations (purple) used to create or evaluate (for AWS) the spatial Antarctic-wide pressure reconstruction. Outlined are the geographic regions used for further comparison, East Antarctica (45°W eastward to 180°, poleward of 66°S), West Antarctica (45°W westward to 180°, poleward of 75°S) and the Antarctic Peninsula (55°W–68°W, 62°S–75°S)



reconstruction for the withheld years. Combining the two predicted reconstructions produced in this manner yields the validation reconstruction. Furthermore, since our reconstruction is based on surface pressure anomalies, this inherently implies that there is a strong vertical correlation between surface pressure anomalies and geopotential height anomalies further aloft, as surface pressure ranges from near 1000 hPa in the Southern Ocean to near 600 hPa in the Antarctic interior. To demonstrate the vertical connection between surface pressure, the correlation between the surface pressure anomalies and geopotential height was calculated separately by pressure level in ERA-Int from 1000 to 500 hPa poleward of 60°S. The minimum squared correlation of surface pressure and geopotential height from all these levels (Supplemental Fig. S1) exceeds 0.6 nearly everywhere poleward of 60°S. This suggests that the use of surface pressure anomalies in our reconstruction does not significantly influence the results and accurately represents the large deviations in surface elevation/pressure poleward of 60°S. However, we do note a few regions of slightly lower correlation across the Ross Ice Shelf and Weddell Sea in some seasons, which likely

reflect high pressure variability near the surface in proximity to steep terrain.

2.3 Climate model simulations

As in Fogt et al. (2017a), we also investigate simulations from the Community Atmosphere Model, version 5 (CAM5) (Neale et al. 2010) for the non-summer seasons. Three core experiments consisting of ten ensemble members each (all members initialized from a pre-industrial control simulation whose initial air temperature was randomly perturbed) are analyzed; these simulations are configured at a 0.9° latitude \times 1.25° longitude horizontal resolution with a finite volume dynamical core and 30 vertical levels. One experiment, here termed 'Ozone Only', is forced with time-varying ozone concentrations, with SSTs, sea ice concentrations and non-ozone radiative forcings held to monthly varying climatologies, and is available over the years 1900–2014. The external forcings without time dependence beyond the seasonal cycle are set to climatological values for the year 1850. As in Fogt et al. (2017a), the ozone forcing is from the Stratospheric-Tropospheric Processes and their Role in Climate (SPARC) dataset (Cionni et al. 2011; Eyring et al.

2013), which is a reconstruction prior to 1978 specifically designed for the use in long-term climate model simulations. The second experiment, available over the years 1874–2014, has prescribed tropical sea surface temperatures, but all radiative forcings including ozone are held to monthly varying climatologies, set to pre-industrial, 1850 values (termed ‘Tropical SSTs + Fixed Radiative’). Observed time-varying tropical SSTs are prescribed over 28°N–28°S, while a monthly varying climatology for SSTs and sea ice concentration is used poleward of 35°S. Between 28° and 35° in both hemispheres, the observed SST anomalies are tapered by adding damped anomalies (linearly weighted by latitude) to the climatologies. The third experiment, available over the years 1880–2014, prescribes sea ice and sea surface temperature the same as the second experiment, but is forced by the full suite of time-varying radiative forcings (including ozone) plus tropical SSTs (termed ‘Tropical SSTs + Radiative’). Further details of these experiments, including a listing of forcing datasets and boundary conditions is provided in Fogt et al. (2017a).

To better understand the influence of uncertainties in the SSTs, we also assess results from two experiments identical to the Tropical SSTs + Radiative experiment, but using the Extended Reconstruction SST version 3b (Smith et al. 2008) and version 5 (Huang et al. 2017) in place of ERSSTv4 (Huang et al. 2015). Finally, the role of extratropical SSTs and sea ice is assessed through a ‘Global SST + Radiative’ experiment in which the full observation-based data set of SSTs and sea ice concentrations is prescribed, using ERSSTv4. In this paper, we use the term “forced response” to refer to the ensemble-mean Antarctic pressure response to SSTs and radiative forcing combined or separately, as indicated in the text.

3 Results

3.1 Reconstruction evaluation

The skill of the spatial surface pressure anomaly reconstruction varies considerably seasonally, as indicated in Table 1, which shows area averaged (for the regions indicated in Fig. 1) skill metrics: reconstruction/calibration and verification squared correlations, and the reduction of error (RE) and coefficient of efficiency (CE) values [see Fogt et al. (2016a) for details about how these metrics are calculated]. The statistics for ‘Total Antarctica’ are the average of the statistics across all three regions, although the reconstruction does extend equatorward to 60°S. As noted in Fogt et al. (2017a), the reconstruction skill is highest in DJF. The focus of this work is on the non-summer seasons, which demonstrate the highest performance in austral winter (JJA), followed closely by austral autumn (MAM). The skill is lowest

Table 1 Spatially averaged reconstruction skill statistics by region (columns) for each season

Statistic	Region			
	East Antarctica	West Antarctica	Antarctic Peninsula	Total Antarctica
DJF				
r^2 recon	0.729	0.755	0.819	0.738
r^2 verif	0.721	0.748	0.808	0.729
RE	0.722	0.739	0.794	0.728
CE	0.714	0.728	0.787	0.720
MAM				
r^2 recon	0.541	0.614	0.630	0.558
r^2 verif	0.537	0.608	0.616	0.553
RE	0.522	0.595	0.559	0.537
CE	0.519	0.590	0.549	0.533
JJA				
r^2 recon	0.653	0.661	0.778	0.660
r^2 verif	0.636	0.651	0.753	0.644
RE	0.643	0.646	0.747	0.648
CE	0.624	0.638	0.731	0.631
SON				
r^2 recon	0.478	0.605	0.759	0.513
r^2 verif	0.469	0.586	0.748	0.502
RE	0.442	0.552	0.724	0.474
CE	0.432	0.536	0.707	0.462

Listed are the squared calibration and verification correlations (r^2 recon and r^2 verif, respectively), the RE, and the CE values

in austral spring (SON), and the seasonal performance of the skill follows that of the individual station reconstructions used in the interpolation (Fogt et al. 2016a). Spatially, the highest reconstruction skill is in the Antarctica Peninsula, also in agreement with Fogt et al. (2016a), and the skill in West Antarctica tends to exceed that in East Antarctica, due to both larger area and lower station density in the latter region. In all cases, the RE and CE values are above 0.40, higher than some monthly Antarctic temperature reconstructions for the period after 1957 (Steig et al. 2009; O’Donnell et al. 2011; Nicolas and Bromwich 2014).

The spatial reconstruction skill is further demonstrated in Figs. 2 and 3, which show maps of the squared calibration correlation and mean absolute error (MAE), respectively, compared to the ERA-Int reanalysis during 1979–2013. In terms of calibration correlations, the lowest skill is seen in all seasons across the high East Antarctic plateau, and regions extending equatorward off the Antarctic coastline, especially in the South Pacific. Correlations with select AWS records that have at least 15 years of data are also displayed in Fig. 2. The AWS evaluations agree well with the values indicated by ERA-Int, despite these values not being included as anchoring points in the reconstruction; the differences arise from

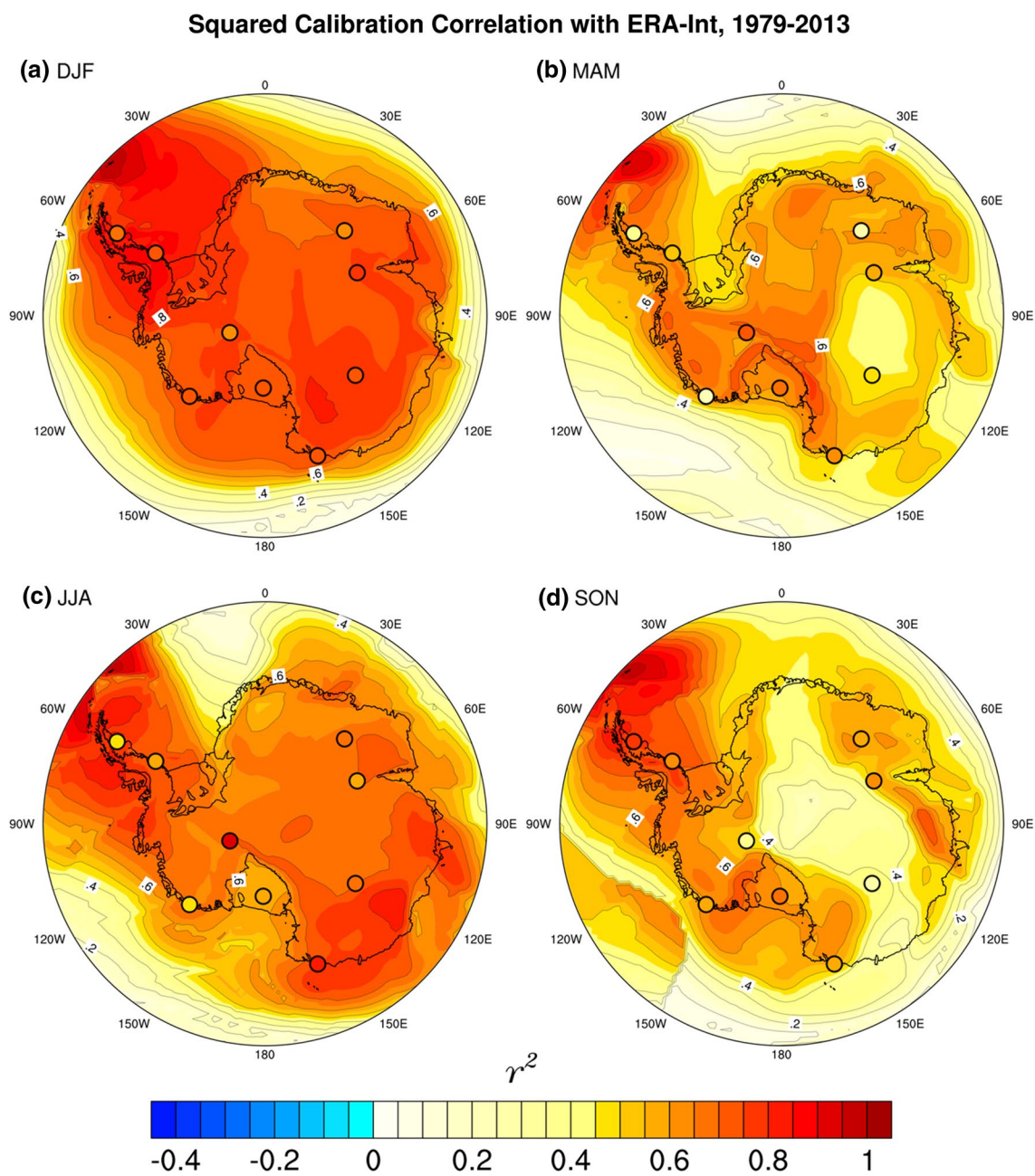


Fig. 2 Squared calibration correlation of seasonal reconstructions with ERA-Interim, 1979–2013. **a** DJF; **b** MAM; **c** JJA; **d** SON

different time periods of data availability over 1979–2013 in the AWS records. The MAE map (Fig. 3) indicates that the reconstruction is generally within 1.5–2 hPa of the ERA-Interim surface pressure anomalies across the Antarctic continent, and that the differences change sharply in the non-summer seasons in the Ross, Amundsen, and Bellingshausen Seas (South Pacific sector). In this region, differences can be as large as 4 hPa on average, and when combined with the low squared correlation values in this region, this clearly indicates that the reconstruction fails to capture the magnitude and patterns of interannual variability in the Amundsen

Sea Low region. This, however, is not surprising given that the closest anchoring stations in the interpolation scheme are along the Antarctic Peninsula, in central West Antarctica, and the western Ross Ice Shelf. The poor performance of the reconstruction in the ASL region is also produced as this region experiences the highest interannual pressure variability across the Southern Hemisphere, termed the ‘Pole of Variability’ (Connolley 1997).

To determine if the lower skill is in the South Pacific is related to limitations in our reconstruction methodology, we employ the same interpolation from 18 grid points using the

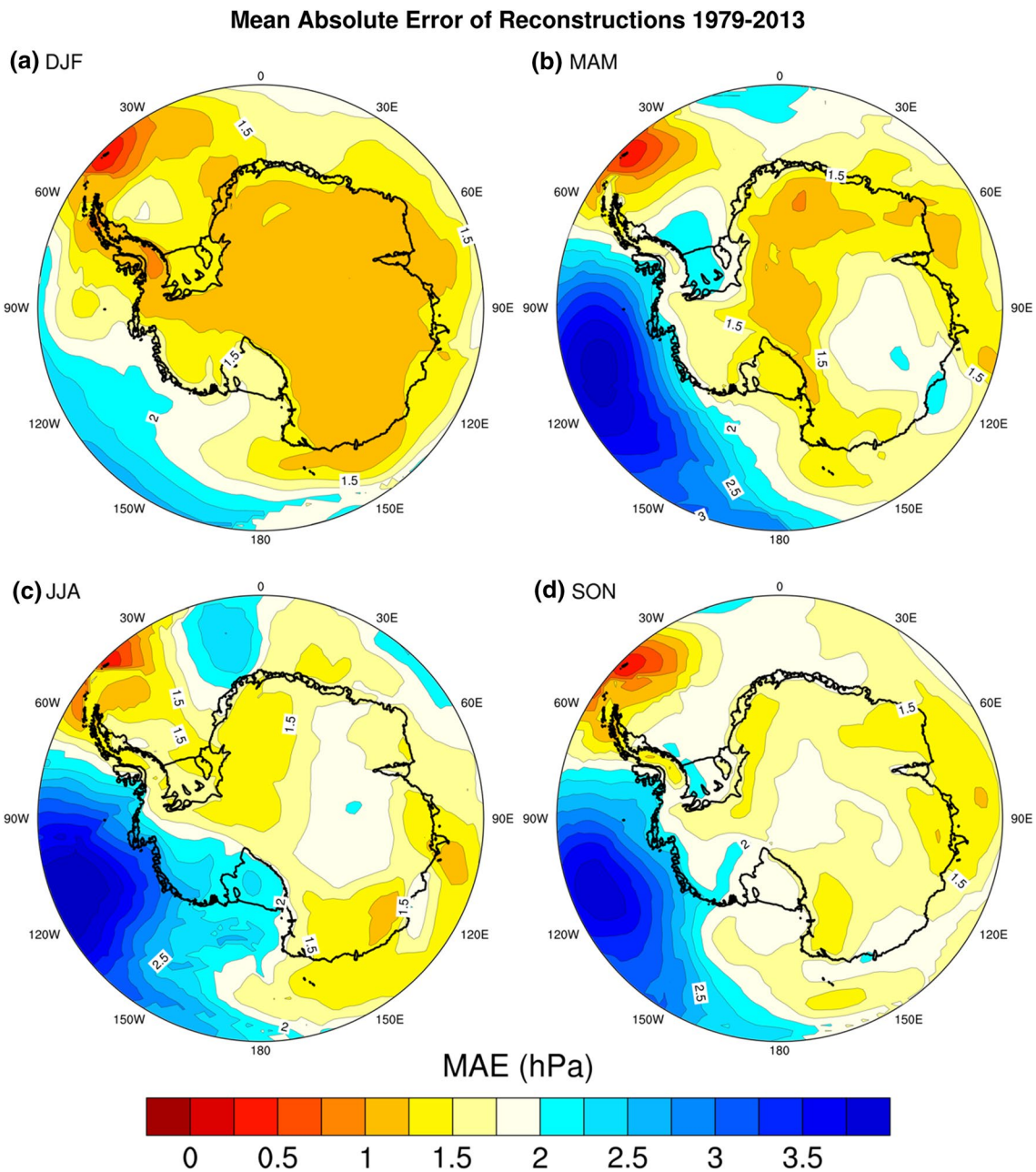


Fig. 3 Mean absolute error (hPa) of seasonal reconstructions compared to ERA-Interim, 1979–2013. **a** DJF; **b** MAM; **c** JJA; **d** SON

first ensemble member in each of the CAM5 experiments (by season) separately. To perform the kriging interpolation, we use the spatial covariance structure in the CAM5 ensemble members during the early and late twentieth centuries (1905–1956 and 1957–2013). As for our verification reconstruction, the spatial covariance field from the early twentieth century is used to perform kriging on the pressure anomalies during the second half of the twentieth century, and vice-versa. Merging these two interpolations in CAM5 produces an independent CAM5-based verification reconstruction, which is then correlated with the full CAM5 data

during 1905–2013. Figure 4 shows the squared verification correlations for each season and CAM5 experiment. Notably, across the entire Antarctic continent, the squared verification correlations from these CAM5 reconstructions exceed 0.90 nearly everywhere, with slightly lower values in portions of East Antarctica. Moving away from the continent, the skill decreases rapidly, especially in the South Pacific. This again reflects the high interannual pressure variability in the Antarctic circumpolar trough which is not captured by the anchoring stations used in the kriging scheme. Furthermore, the fact that the CAM5 verification squared correlations are

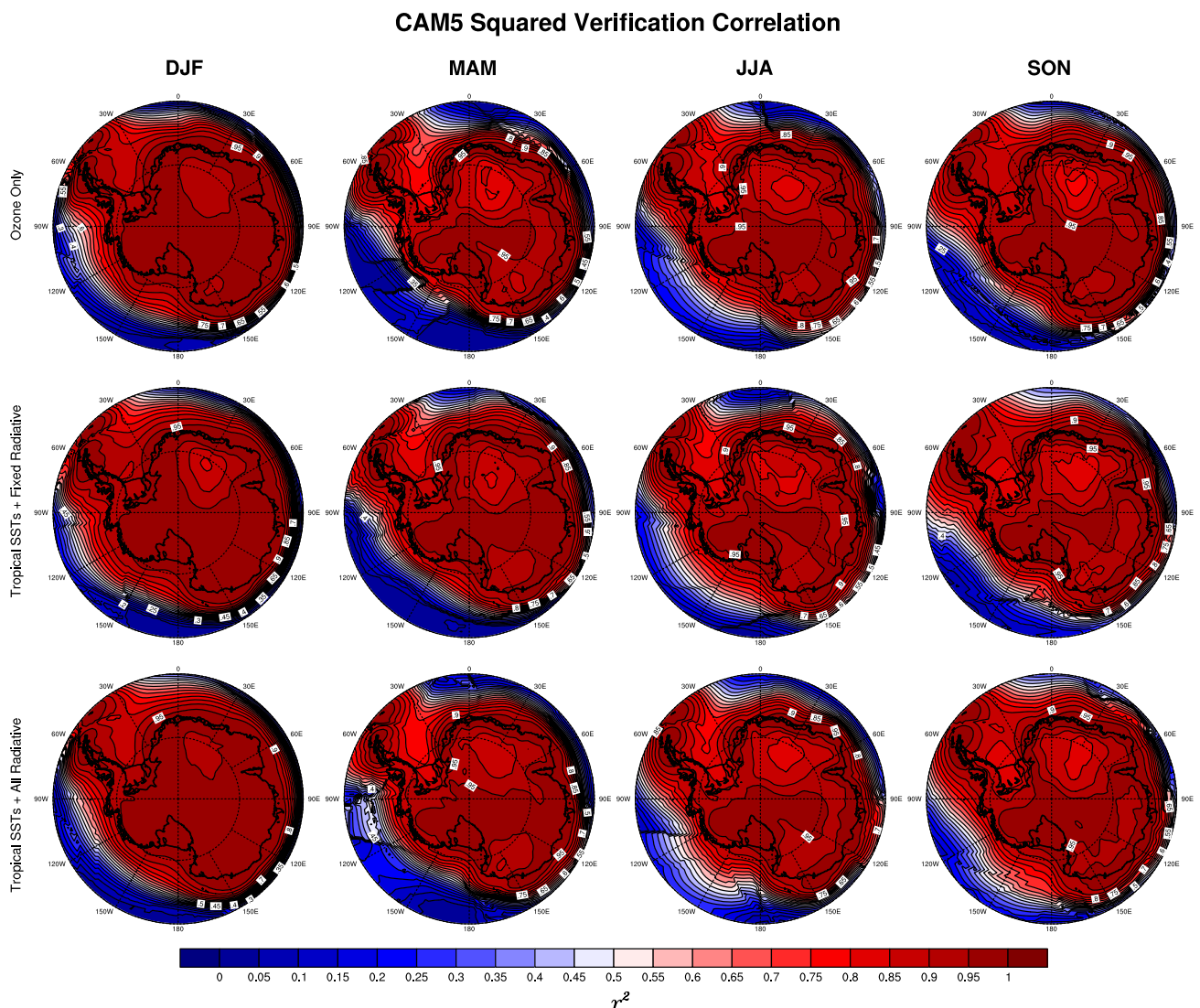


Fig. 4 CAM5 reconstruction verification squared correlation by CAM5 experiment (rows) and seasons (columns). See text for details

very high across the continent provides further support that the spatial covariance pattern changes little across Antarctica throughout the twentieth century, despite changes in applied forcing across the various experiments. We therefore conclude that using only the 1979–2013 ERA-Int spatial covariance structure to perform our reconstruction does not cause significant error, as this pressure covariance structure does not change in the twentieth century.

Figures 2, 3 and 4 indicate that a primary reason of low reconstruction skill across the Antarctic continent is due to station reconstruction skill used as anchoring points (Fogt et al. 2016a), while the error in the Southern Ocean is primarily due to the lower performance of the kriging interpolation scheme. Given the latter, the reconstruction does not provide a good estimate of the long-term pressure variability of the ASL, and even further attempts to improve the skill in

this area by adding additional anchor points of reconstructed ERA-Int gridpoint values only slightly improved the reconstruction performance (not shown). Nonetheless, the reconstruction skill is well above simply using the climatological mean across the entire ice sheet, and when area-averaged, across the entire domain poleward of 60°S. Given this skill, we now assess the seasonal Antarctic pressure variability throughout the twentieth century.

3.2 Antarctic pressure variability during the twentieth century

Area-averaged pressure anomaly time series (Fig. 5) reflect the temporal similarities between ERA-Int and the reconstruction (note that the correlations in Fig. 5 in each plot are based on the area-averaged pressure anomaly time series, not

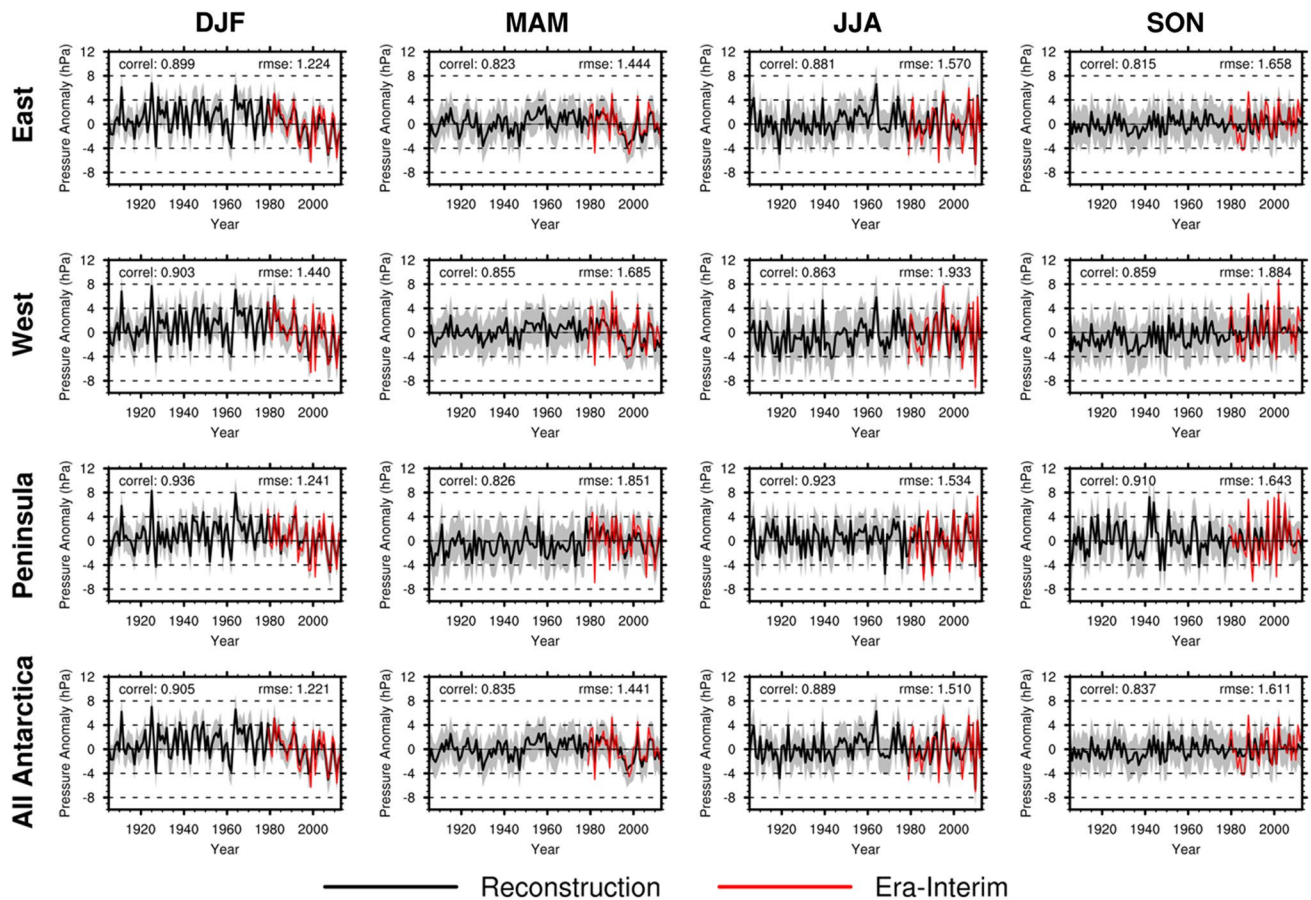


Fig. 5 Seasonal (by columns) time series of the reconstructed (in black) area averaged pressure anomalies for regions (by row) identified in Fig. 1. All of Antarctica is the average of the East, West, and Antarctic Peninsula time series. The 95% confidence intervals about the reconstructed data are shown as the gray shaded region in each

panel, calculated as ± 1.96 times the standard deviation of the residuals between the reconstruction and ERA-Int data during the period of overlap. The ‘correl’ and ‘RMSE’ values in each panel are the correlations and root mean squared error, respectively, of the reconstruction and ERA-Int time series (red)

the area-averages of the squared correlations at each grid-point as in Table 1). The only season with a negative pressure trend during the entire twentieth century is in DJF, most marked in East Antarctica (Fogt et al. 2017a). While MAM shows a negative trend in East and West Antarctica from 1980 to 2000, after 2000 the pressure anomalies weaken, and similar other negative pressure anomalies comparable to the late twentieth century values occur earlier in the reconstruction. The regionally-averaged time series also indicate that throughout the twentieth century, both JJA and SON are marked with strong interannual pressure variability, especially outside East Antarctica. The reconstruction captures this fairly well in JJA (with slightly higher correlations), but shows less skill in SON at capturing the frequent extreme deviations and the reconstruction variability is considerably dampened outside the Antarctic Peninsula. In both JJA and SON, root mean squared error values are the largest in West Antarctica, where the variability indicated by ERA-Int is the largest. Notably, the reconstruction shows

similar interannual variability across both West Antarctica and East Antarctica, especially in MAM, in agreement with ERA-Int. The larger variability in ERA-Int compared to the reconstruction, especially in SON, reflects the fact that the variability in these station reconstructions used as anchoring points in the kriging interpolation is slightly dampened compared to observations especially in coastal East Antarctica and the Antarctic Plateau (Fogt et al. 2016a).

To investigate the potential drivers of twentieth century Antarctic pressure variability and trends, we employ the CAM5 model using the three experiments spanning the entire twentieth century and compare these to the reconstruction seasonally. Figure 6 shows the 60°S–90°S area averaged pressure anomaly time series from the CAM5 ensemble mean for each season (columns) and experiment (rows). The gray shading represents the range of all ten ensemble members for each experiment, and the correlation values are calculated between the CAM5 ensemble means and the reconstruction during the full period of

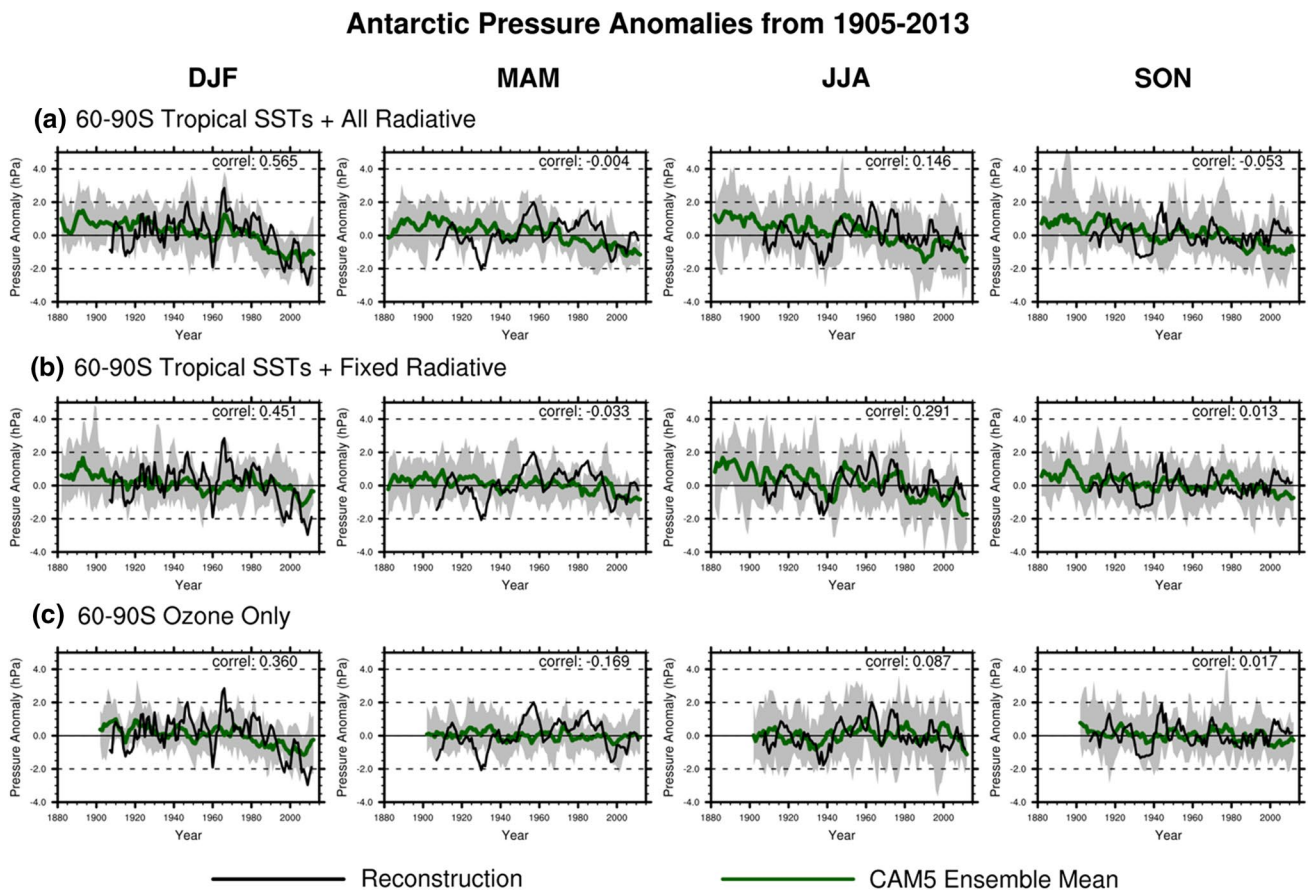


Fig. 6 Seasonal (by columns) time series of pressure anomalies averaged over 60°S–90°S for the reconstruction (black line) and CAM5 ensemble mean (dark green line). The gray shading corresponds to the range of the 10 CAM5 ensemble members for each experiment. All data have been smoothed with a 5-year running mean. **a** Top row,

CAM5 Tropical+All Rad; **b** middle row, CAM5 Tropical+Fixed Rad; **c** bottom row, CAM5 Ozone only. The ‘correl’ value is the correlation between the reconstruction and the CAM5 ensemble mean in each panel during 1905–2013

overlap. These correlations only have substantial magnitude in DJF, highlighting the emergence of a forced response in the observations, as discussed in Fogt et al. (2017a). For the other seasons, which is the focus of this study, the correlations are weaker and none are statistically significant. Unless the forced response is very strong relative to the internal variability, nature (as approximated by the reconstruction) should not be expected to follow the ensemble mean. For nearly all time periods in every season, the reconstructed time series lies within the ensemble spread of the CAM5 experiments (especially the Tropical SSTs + All Radiative Experiment), indicating that the reconstructed variability is consistent with the major known climate forcings of the twentieth century, and that the model’s estimates of internal variability are reliable.

Figure 7 displays anomaly composites (from the 1905–2013 mean) for three independent 30-year periods of interest based on the area-averaged time series in Fig. 5 that collectively represent the majority of the twentieth

century pressure variability. The stippling in Fig. 7 indicates regions where the 30-year mean is statistically different from zero at $p < 0.05$, based on a single-mean student’s t test; cross-hatching indicates regions where the composite mean anomaly is different from zero after including the uncertainty in the reconstruction. The spatial reconstruction uncertainty was calculated in a manner analogous to the uncertainty envelope displayed in Fig. 5; at each grid point the uncertainty is taken as ± 1.96 times the standard deviation of the residuals between the ERA-Int and reconstruction. In addition, it should be noted that the spatial reconstruction anomalies are sensitive to the background covariance field in ERA-Int used in the interpolation. Therefore, the reconstruction surface pressure anomaly contour lines are more strongly tied to the terrain than they would likely be in a data-rich environment, especially along the Ross Ice Shelf (reflected also in Fig. S1), but the general pattern over the continent is consistent with ERA-Int during overlap (as shown in Figs. 2, 3).

Seasonal Reconstruction Anomaly Composites

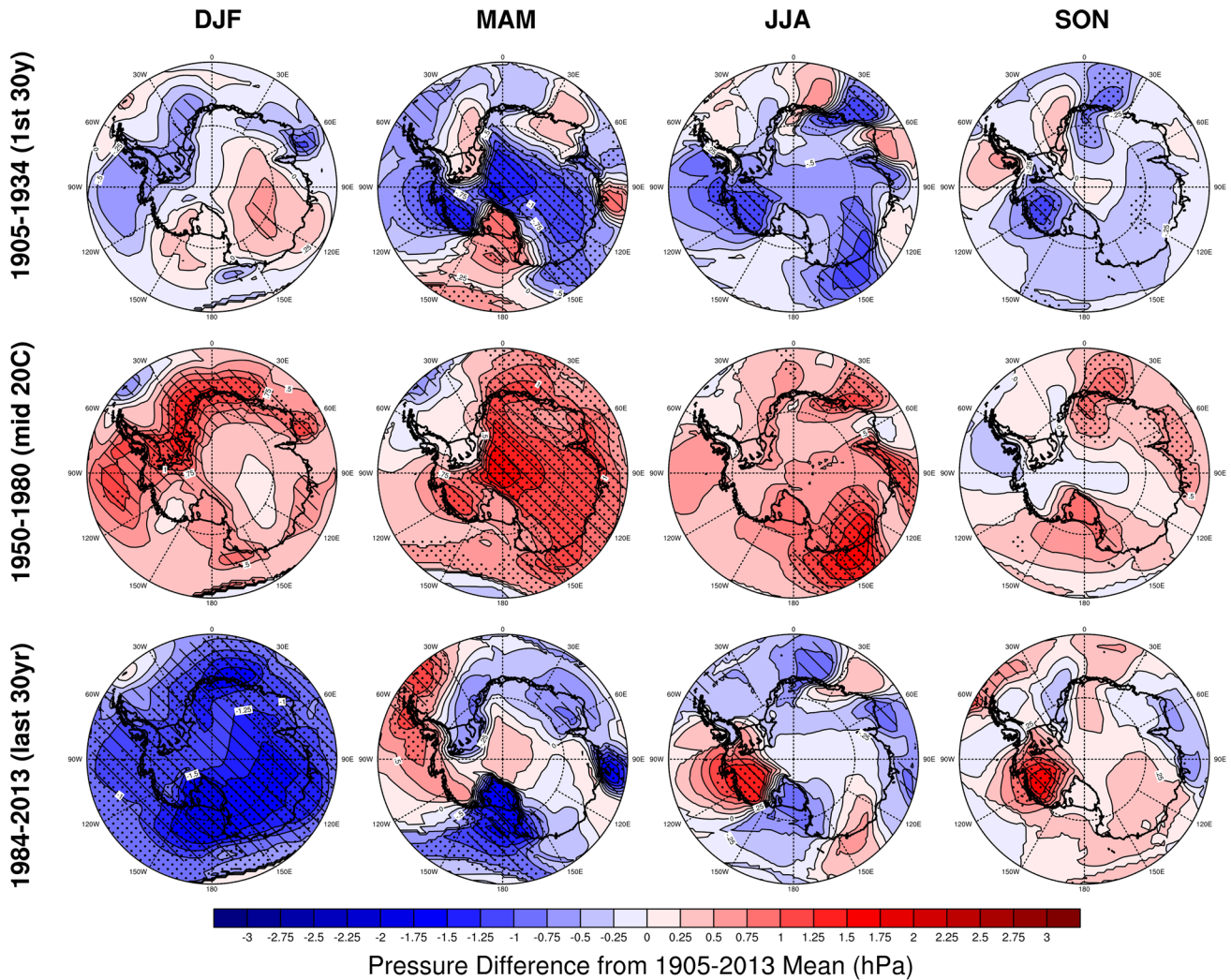


Fig. 7 Seasonal (by columns) anomaly composites of the reconstruction data for 1905–1934 (top row), 1950–1980 (middle row), and 1948–2013 (bottom row). Shading corresponds to the mean anomaly (from the 1905–2013 mean) during the 30-year period. The stippling indicates average anomalies that are statistically different from zero

From the anomaly composites, the first part of the twentieth century (Fig. 7, top row, 1905–1934) was marked with below average pressures, which switched to above-average pressure anomalies in the 1950–1980 period; many of the pressure anomalies in both periods are statistically significant (stippling) but only some of the anomalies emerge beyond the reconstruction uncertainty (cross-hatching) in SON. The change from negative pressure anomalies in the early twentieth century to positive anomalies in the mid twentieth century across the Antarctic continent is most widespread and robust during MAM; only a few locations display significant (when accounting for both interannual variability and reconstruction uncertainty) changes in JJA.

at $p < 0.05$, while cross-hatched regions indicate average anomalies that are different from zero when the reconstruction uncertainty is included. The reconstruction uncertainty is calculated at each grid point as 1.96 times the standard deviation of the residuals between the reconstruction and ERA-Interim during 1979–2013

During 1984–2013, the last 30 years of the reconstruction, significant negative pressure anomalies poleward of 60°S are only seen in DJF. In MAM there are also significant negative pressure anomalies but primarily on the Ross Ice Shelf and portions of coastal East Antarctica which also are different from zero based on the reconstruction uncertainty in these regions, but the Peninsula region stands in contrast with significant positive pressure anomalies during this period.

Composite anomalies were similarly constructed for every CAM5 ensemble member. Across the three main experiments analyzed in Fig. 6 and in Fogt et al. (2017a) as well as the additional SST sensitivity experiments, this constitutes 60 ensemble members. An additional 60 pseudo

ensemble members were constructed by removing the experiment's ensemble mean from each ensemble member (e.g., the 'Tropical SST + All Radiative' ensemble mean was removed from each of the ten corresponding ensemble members, and similarly for the other five experiments). This step acknowledges the dominance of internal atmospheric variability as discussed previously, as well as uncertainties in the forced response to SSTs (discussed later). Each ensemble composite was compared to the reconstruction composites in Fig. 7 separately by calculating the weighted (by cosine

of the latitude) pattern correlation and RMSE values (after masking regions where the reconstruction error is larger than 2 hPa from Fig. 3). Figure 8 displays the ensemble member composite anomaly that corresponded best to the reconstruction anomaly composite (determined here by the lowest RMSE value). In each panel, the name of the CAM5 experiment is provided as well as the pattern correlation and RMSE value; a "***" indicates cases where the ensemble member that best aligned with the reconstruction anomaly composite was from an experiment with the ensemble

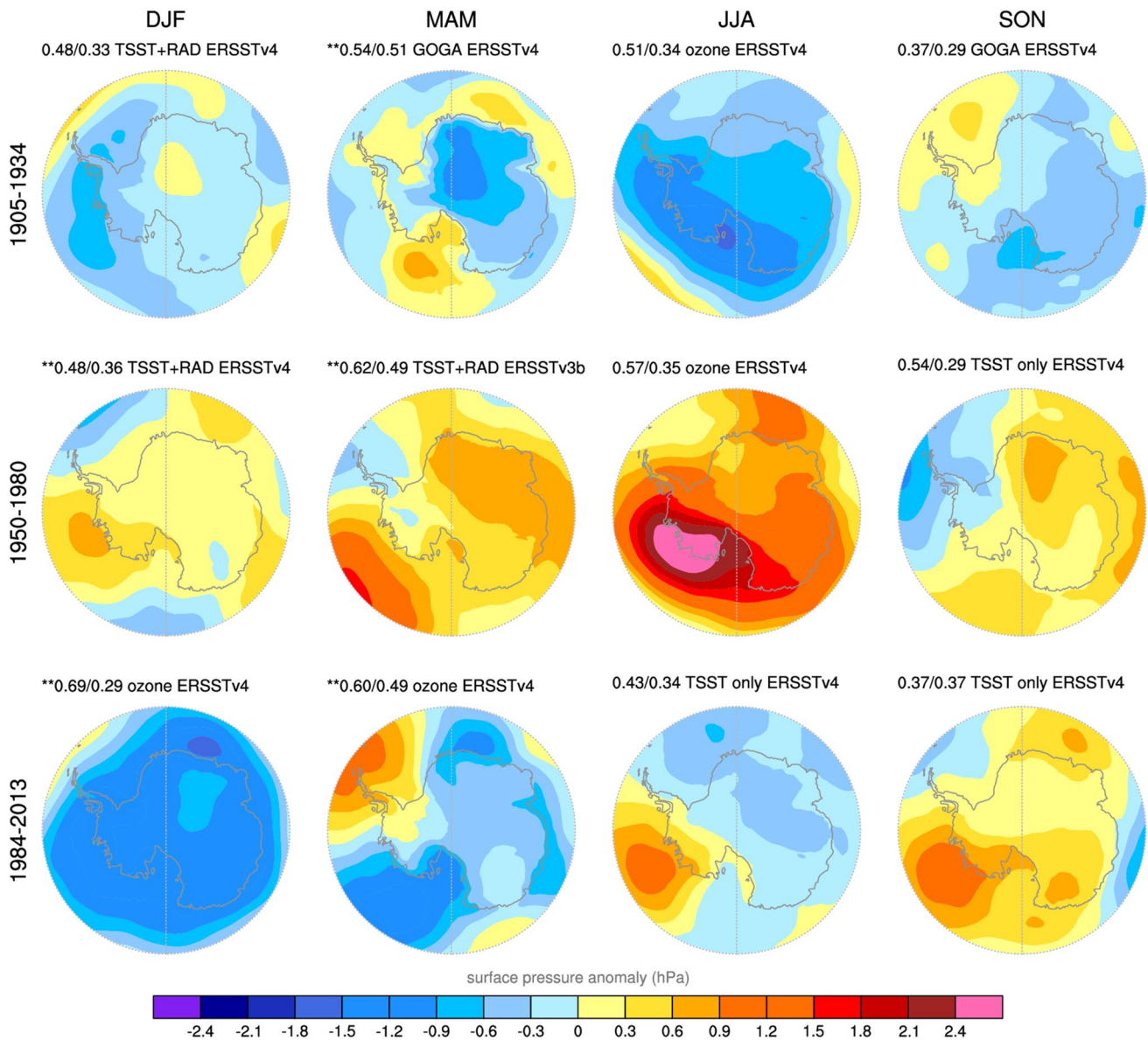


Fig. 8 Seasonal (in columns) anomaly composites for individual ensemble members across the various CAM5 experiments for the same time periods as in Fig. 7 (in rows). The numerical values in each panel are the pattern correlation and the RMSE between the ensemble member and the reconstruction anomaly composite for regions where the reconstruction MAE is less than 2 hPa (Fig. 3). The

ensemble members chosen for display were those that had the lowest RMSE values. The ** indicates anomalies based on the original CAM5 experiment, while those without ** indicate composites constructed with the ensemble mean (forced response) removed. In each panel, the name for the CAM5 experiment for the ensemble member that best aligned with the reconstruction is given

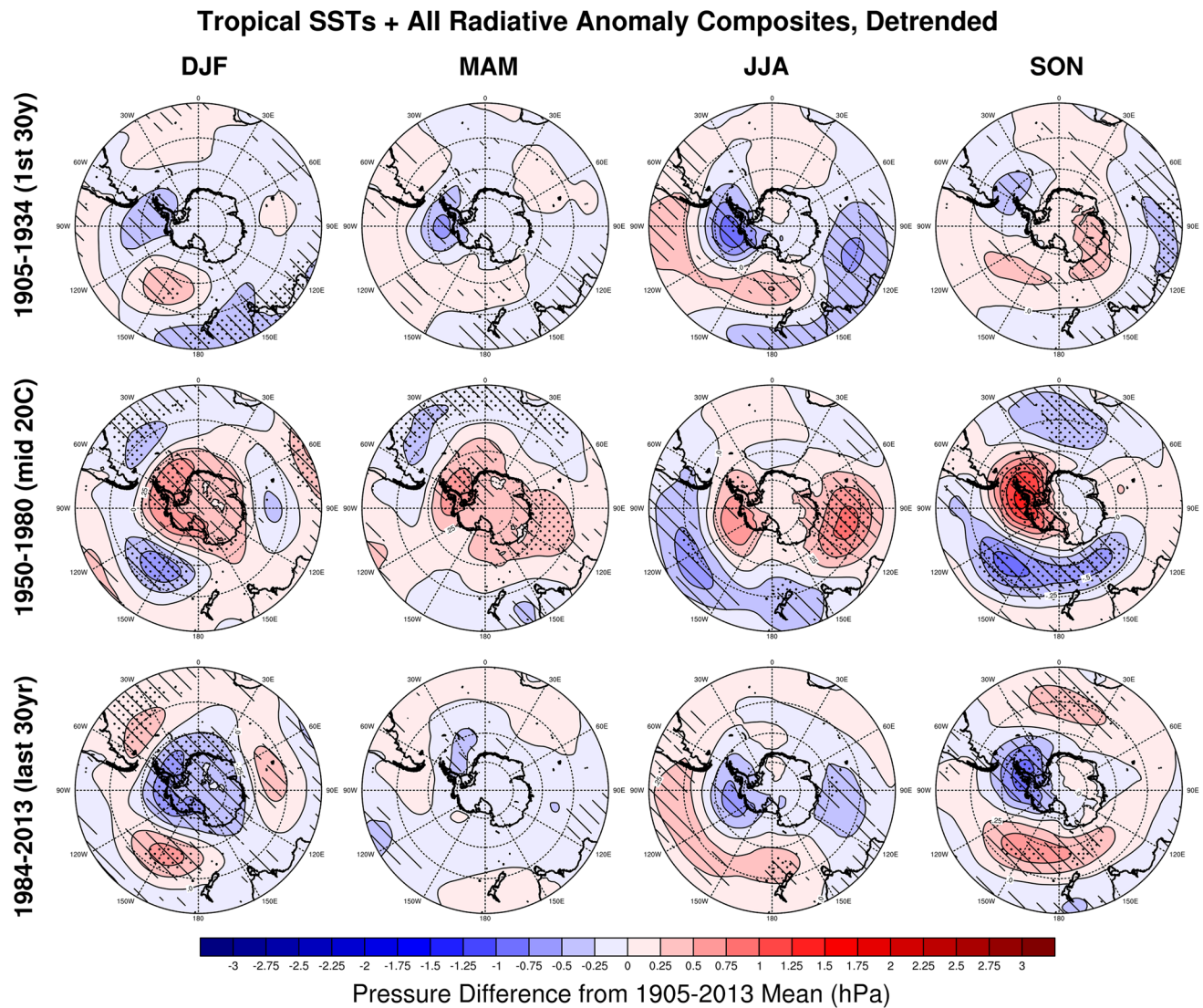


Fig. 9 As in Fig. 7, but based on the ensemble mean from the CAM5 Tropical SST+All Rad experiment with the long-term (1905–2013) trend removed. Stippling indicates regions where the composite mean anomaly is significantly different than zero at $p < 0.05$. Cross hatch-

ing in each panel indicates regions where at least nine out of the ten ensemble members agree on the sign of the pressure anomaly for each 30-year period

mean included, while the other anomaly composites were selected from experiments patterns that have the ensemble mean removed. For completeness, composites based on the detrended ensemble mean from the CAM5 Tropical SST + All Radiative experiment are shown in Fig. 9.

Figure 8 provides important information that sheds light on the processes that govern Antarctic pressure variability throughout the twentieth century. First, the highest pattern correlations and lowest RMSE and therefore the best agreement between the reconstruction and CAM5 experiments are found in DJF. Further, the agreement is best when the ensemble mean is retained, and for the Ozone Only experiment after 1984 and Tropical SSTs + All Radiative experiment prior to this, reflecting the important role of ozone

depletion on recent summer Antarctic pressure trends and the secondary role from tropical SSTs as discussed in Fogt et al. (2017a). Although the RMSE values are somewhat larger, the influence of a forced response in MAM in the twentieth century Antarctic pressure variability is also discernable. Consistently for all time periods, the ensemble members that agreed the best with the reconstruction were those where the ensemble mean was retained. Specifically, tropical SSTs and external radiative forcing play an important role in generating the negative pressure anomalies in the early twentieth century and the positive pressure anomalies across the Antarctic continent in the mid twentieth century. The detrended ensemble-mean composites (Fig. 9) still show positive pressure anomalies in the mid twentieth century, but

they are relatively weak. The anomalies in MAM, therefore, can be interpreted as the sum of a forced response and internal atmospheric variability. This interpretation is consistent with other work showing an important role of tropical SST variability on the Antarctic pressure trends in MAM since 1979 (Ding and Steig 2013), and on related trends in zonal winds (Schneider et al. 2015). Moreover, it is consistent with the reconstruction itself, in that the pressure anomalies across much of the Antarctic continent are significant above the background interannual variability and the reconstruction uncertainty.

In contrast to MAM, Fig. 8 reveals that the best match with the reconstruction for all time periods in JJA and SON is when the ensemble mean is removed from each ensemble member. Figure 9 further demonstrates a degree of similarity between the reconstruction and CAM5 composites based on detrended pressure anomalies, with positive pressure anomalies in the mid twentieth century and negative pressure anomalies in the early twentieth century. Since the removal of the long-term trend or ensemble mean (i.e., the forced response) improves the agreement between the reconstruction and model simulations, this suggests that either the CAM5-forced trend in these seasons is too large (Fig. 6), or that the pressure anomalies in these seasons are dominated by large internal variability. The dominance of internal variability fits with the results of the reconstruction discussed above—that the pressure anomalies in JJA and SON are not significant in most parts of the Antarctic continent when interannual variability and reconstruction uncertainty are taken into account (Fig. 7).

The long-term negative trends in JJA and SON in the ensemble means of the experiments that include tropical SSTs (Fig. 6a, b) underscore some limitations of the experiments and comparing them to the reconstructions. The simulated spatial patterns of the Tropical SST + All Rad experiment with the long-term trend retained (Fig. S3) show a SAM-like response in all seasons, with an embedded wave-train in the Pacific sector in MAM, JJA and SON. The SAM-like response has been seen in other SST-forced experiments with other models and attributed to the long-term warming trend in tropical SSTs (Staten et al. 2012). The embedded wave-train resembles the extratropical circulation response to interannual La Niña variability (Turner 2004; Clem et al. 2016). This pattern likely arises from the east–west gradient of SST trends in the tropical Pacific. In ERSSTv4, like many similar datasets, the western Pacific warms more than the eastern Pacific during the twentieth century. This gradient is uncertain and difficult to constrain from observations (Deser et al. 2010; Solomon and Newman 2012). Nonetheless, it is persistent across all recent generations of the ERSST analysis, and all of the SST-forced experiments show the SAM-like pattern and the wave-train response in the Southern Hemisphere high-latitudes, albeit much weaker when

the long-term trend is removed (Figs S4–S8). In particular, the Global SST + Radiative experiments exhibit somewhat weaker trends when integrated over 60°S–90°S, owing to a stronger stationary wave response in the high latitudes (Fig. S8). Again, the reduced agreement between the reconstruction and the ensemble-mean only demonstrates that internal atmospheric variability dominates at high latitudes. However, the forced response in the model simulations could be too strong, owing to uncertainties in the SSTs and/or model physics. As noted earlier, the reconstruction may not adequately capture pressure variability in the Pacific sector where the tropical teleconnections are strongest, challenging the discernment of a forced response in JJA and SON.

To illustrate the temporal evolution of Antarctic pressure trends, Fig. 10 displays linear pressure trends for the 60°S–90°S domain, as well as East and West Antarctica separately for various time periods of at least 30-years (as indicated by the plot axes, following Fogt et al. 2017a) from the reconstruction. For the non-summer seasons, there are positive pressure trends for most regions up until around 1990, regardless of the start date. Most of these trends reach statistical significance at $p < 0.05$, and peak during 1950–1970, as reflected in the middle row of the anomaly composites in Fig. 5. After 1950, MAM shows negative pressure trends, which are a combination of strong positive pressure anomalies across the Antarctic continent in the 1950–1980 period and some regions of negative pressure anomalies during the 1984–2013 period (Fig. 7). However, the recent negative pressure trends in MAM are weaker (in an absolute sense) and less persistent than the positive pressure trends before, highlighting an important role of multi-decadal Antarctic pressure variability in this season. In JJA, East Antarctica is the only region to show significant ($p < 0.05$) negative pressure trends in the twentieth century, but they are sensitive to the starting year (1950s in general). In addition, these negative pressure trends in winter are overshadowed by earlier positive pressure trends, which are more persistent and greater in absolute magnitude. In SON, the reconstruction indicates only in West Antarctica are there significant positive trends, which extend throughout the entire twentieth century but reach their greatest magnitude during the middle twentieth century, as suggested by the composites in Fig. 7. In West Antarctica, significant long-term positive trends are also seen in JJA.

4 Discussion

To explore other possible mechanisms for the twentieth century Antarctic pressure trends and variability, time trends as in Fig. 10 are plotted for various climate indices known to affect Antarctic climate in Fig. 11. Here the ‘Fogt’ SAM index reconstruction (Fogt et al. 2009), from 1905 to 2005,

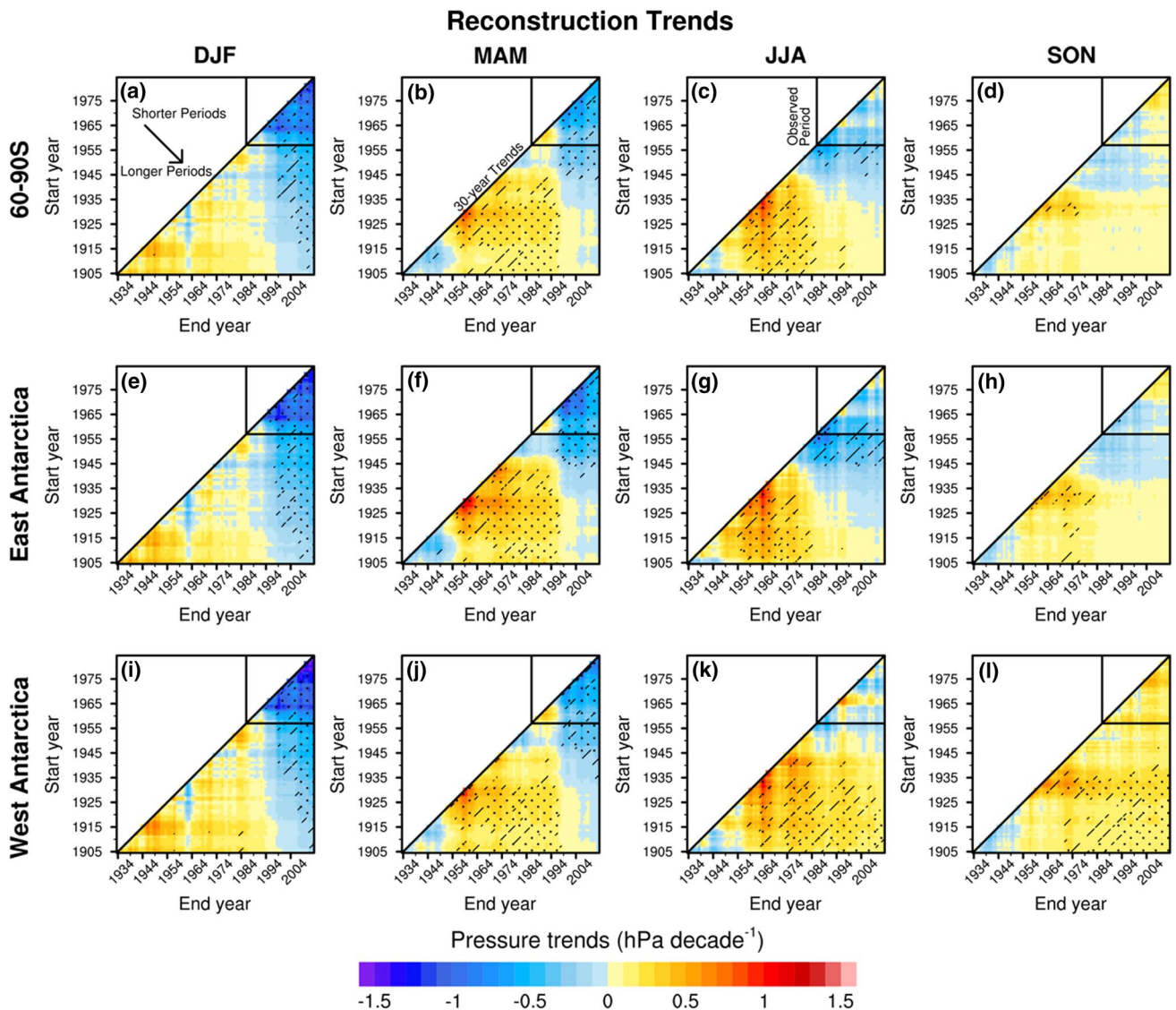


Fig. 10 Seasonal (by column) pressure trends averaged for the 60°–90°S (top row), East Antarctica (middle row), and West Antarctica (bottom row). The trends are calculated for different starting (indicated by y-axis values) and ending (indicated by x-axis values) years, and are only shown if there are at least 30 years of data used to calculate the trends. Diagonal cross-hatching and stippling indicate trends

significantly different from zero at $p < 0.10$ and $p < 0.05$, respectively. Trends calculated using the longest data are found at the bottom right of each panel (as indicated in **a**), and the diagonal area where shading starts corresponds to trends calculated using exactly 30 years of data (as indicated in **b**)

is merged with the observationally-based Marshall (2003) SAM index through 2013, and inverted to match the Antarctic pressure anomaly trends (top row, Fig. 10). While the SAM index reconstruction is based only on midlatitude pressure, we note that there is some overlap in observed pressure records used in the Marshall (2003) SAM index after 1957 with individual station reconstructions from Fogt et al. (2016a) that were the anchor points for our spatial reconstruction. We also investigate tropical indices, namely the Niño 3.4 sea surface temperatures (based on the ERSSTv4 dataset; Huang et al. 2015) and the Southern Oscillation

Index from the Australian Bureau of Meteorology (<http://www.bom.gov.au/climate/current/soi2.shtml>), which starts in 1876. Lastly, given its potential role in recent warming across West Antarctica and sea ice loss (Clem and Fogt 2015; Meehl et al. 2016; Purich et al. 2016), we also investigate the unfiltered monthly Interdecadal Pacific Oscillation based on ERSSTv4 data (Henley et al. 2015).

The inverted SAM index trends are strongly consistent with the observed pressure trends (Fig. 10), especially over 60°S–90°S and East Antarctica, although the reconstruction often shows stronger trends that are both more significant

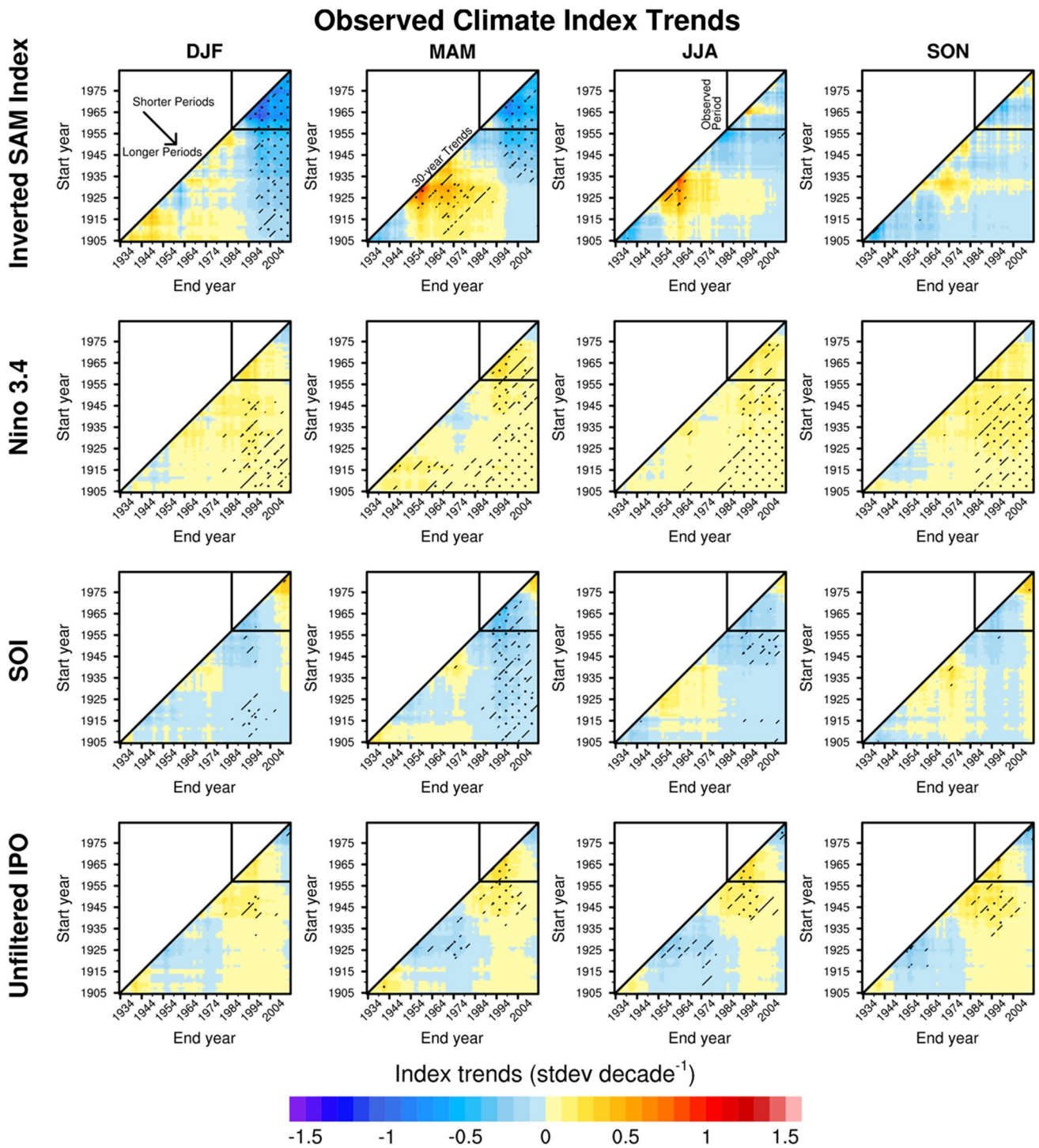


Fig. 11 As in Fig. 10, but for various seasonal mean century-length climate mode indices: Fogt SAM index reconstruction (top row); Niño 3.4 SST index (second row); SOI (third row); unfiltered IPO (bottom row)

and more persistent than the SAM index. The strong similarity in Fig. 11 with the inverted SAM index trends is not surprising, given that the SAM index is based on mean sea level pressure data and is highly correlated with pressure south of 60°S (Marshall 2003); the reconstruction adds

further information beyond the SAM index by examining regional patterns of pressure variability and change across the Antarctic continent (Figs. 7, 8, 9). Due to the global warming signal, the Niño3.4 trends are positive throughout the whole time period, but the SOI suggests a period

of positive trends in the mid-twentieth century, which indicates a trend toward more La Niña (LN) events. Combined with the negative SAM index trends (inverted from top row), this suggests a LN/SAM- combination throughout much of the middle twentieth century, which tends to produce weak anomalies in the ASL region and positive anomalies over the continent with regional variations (Stammerjohn et al. 2008; Fogt et al. 2011; Wilson et al. 2016). This out-of-phase relationship with SAM/ENSO is common throughout much of the early twentieth century, as the inverted SAM index trends mirror those of the SOI, suggesting a negative correlation between the two. However, given that the ENSO signal near Antarctica is strongest in the vicinity of the ASL (Turner 2004) and the reconstruction skill is lowest in this region (with highest MAE, Figs. 2, 3), the reconstruction may miss much of this impact by providing a more robust signal across the Antarctic continent. Similarly, the IPO suggests also an opposing relationship between the SAM and tropical variability, as this index displays a negative trend during the mid-twentieth century (as observed recently), which is consistent with a more La Niña-like state in the equatorial Pacific and therefore lower pressure anomalies across the Pacific sector of Antarctica in the early-mid twentieth century (opposing the SAM index trends). Detrended correlations between the climate mode indices and the reconstruction averaged over 60°S–90°S produce similar results (Supplementary Fig. S9) as the climate index trends. In particular, the correlations show a strong persistent SAM relationship with Antarctic pressure in all seasons throughout the twentieth century. In contrast, the correlations only show a connection of Antarctic pressure variability to tropical patterns of variability in the summer when the last 20 years are included (i.e., correlations that end after the 1990s), with only marginally significant ($p < 0.10$) and short-lived correlations in other seasons. Combined, the correlations with the reconstruction and the climate index trends demonstrate a strong relationship between the SAM and Antarctic pressure variability throughout the twentieth century.

In austral summer and autumn, comparison of the reconstruction with the model results suggests a discernable role for SSTs and external radiative forcing in driving multidecadal pressure variability over Antarctica during the twentieth century. The reconstructed anomaly patterns best match the model results when the latter include the ensemble-mean, forced response. Internal atmospheric variability still plays a large role, as the best-matched simulated patterns include both the forced response and internal variability. In winter and spring, our results suggest that the forced response of Antarctic pressure anomalies to SSTs and external radiative forcing is not detectable on the multi-decadal to centennial timescale. This is consistent with the large pressure variability in these seasons and the relatively low significance of the reconstructed anomalies. Nonetheless, it also points

to one of the key limitations of the reconstruction, in that the skill is lowest in the South Pacific, exactly where the model shows the largest forced response. Model boundary conditions also have important limitations. The implications of the tropical SST gradients have been discussed previously, and we also note that the Antarctic sea ice anomalies (prescribed only in the Global SST + All Radiative experiment; all other experiments used climatological sea ice) are highly uncertain and could play a role in Antarctic decadal-scale pressure variability. Taken together, these results do not mean that the model is flawed; rather, they underscore the key role of internal atmospheric variability even in multi-decadal pressure trends, as well as the importance of improving the observation-based boundary conditions.

5 Conclusions

This paper has presented new seasonal spatially complete reconstructions of Antarctic pressure anomalies extending back to 1905, poleward of 60°S. The skill of this reconstruction varies seasonally, primarily based on the varying skill of individual station pressure reconstructions from Fogt et al. (2016a, b) on which the interpolated spatial pressure field analyzed here is based. The main focus of this work is to evaluate non-summer pressure variability across the twentieth century, as the summer season, where external forcing is stronger and the reconstruction skill markedly higher, was the focus of prior work (Fogt et al. 2017a).

Although the reconstruction performance is lower outside of austral summer, the skill is still sufficient that it provides new information on the range and scope of historical pressure variability over Antarctica. Seasonally, the reconstruction aligned the best with ERA-Int in austral winter, with lower but nearly equal skill in both autumn and spring. The performance drops markedly away from the Antarctic continent, particularly in the vicinity of the Amundsen Sea Low and across the South Pacific, where high interannual variability and the lack of nearby stations are the primary sources of the spatial reconstruction error. From regionally averaged pressures across the continent, it was determined that only in summer are there significant pressure trends across Antarctica over the entire twentieth century. The autumn and winter seasons were particularly marked with significant positive pressure trends throughout the middle of the twentieth century across nearly the entire Antarctic continent, while the negative pressure trends in the observations during autumn (Turner et al. 2005) only emerge as significant after 1945. Nearly all of the pressure trends and their variability are consistent with changes in the SAM index throughout the twentieth century, with a possible smaller role played by variability in the IPO.

To investigate potential forcing mechanisms and evaluate the reconstruction in more detail, a suite of climate model simulations with various combinations of prescribed SSTs and radiative forcings were examined. These simulations clearly show the importance of ozone depletion in the summer, and possibly to a limited extent in MAM. The model experiments also suggest that the positive pressure anomalies and trends in the middle of the twentieth century seen in the reconstruction result primarily from internal atmospheric variability, as the reconstruction largely falls within the ensemble spread in all seasons. However, the analysis here suggests there is a likely connection to tropical SSTs in MAM throughout the twentieth century. Uncertainty in the model experiment, particularly in the east–west tropical Pacific SST gradient that strongly influences teleconnections, could contribute to the lack of clear evidence for SST responses in the other seasons. Moreover, the model experiments are also limited by the fact that they do not include Antarctic sea ice variations, which likely influenced Antarctic atmospheric circulation throughout the twentieth century, but which has poor observational coverage in the early and middle twentieth century.

Future work is needed to continue to improve the scientific understanding of Antarctic climate throughout the twentieth century. The reconstruction provides a better estimate of pressure variability over Antarctica in the twentieth century, especially compared with century-length atmospheric reanalysis products (Schneider and Fogt 2018). However, it is unable to provide a reliable estimate of pressure variability and change in the vicinity of the Amundsen Sea Low, despite the important role of the ASL in ongoing Antarctic climate change (Raphael et al. 2016). Historical estimates of sea ice prior to the early 1970s would also be critical to understand how ice–ocean–atmosphere feedbacks have changed over the twentieth century, and to better place the large Antarctic climate variability in a longer context (Jones et al. 2016). Finally, improvement in the performance of climate models over Antarctica will be valuable to pinpoint the role various mechanisms play in Antarctic climate throughout the twentieth and into the twenty-first centuries.

Acknowledgements Data from both the station-based and spatial pressure reconstructions are available from figshare at the following URLs: <https://doi.org/10.6084/m9.figshare.3412813> (station reconstructions) and <https://doi.org/10.6084/m9.figshare.5325541> (spatial reconstructions). Data for the climate model simulations may be downloaded by following the links at <http://www.cesm.ucar.edu/experiments/cesm1.1/LE>, or by contacting the authors. RLF, CAG, LNC and MJG acknowledge support from the National Science Foundation (NSF), Grant PLR-1341621, while DPS acknowledges support from NSF Grant PLR-1341527. The Climate Variability and Change Working Group of the Community Earth System Model led the production of the CAM5 experiments with time-varying tropical or global SSTs and

time-varying radiative forcing. This material is based upon work supported by the National Center for Atmospheric Research, which is a major facility sponsored by the National Science Foundation under Cooperative Agreement no. 1852977.

References

- Cionni I, Eyring V, Lamarque JF et al (2011) Ozone database in support of CMIP5 simulations: results and corresponding radiative forcing. *Atmos Chem Phys* 11:11267–11292. <https://doi.org/10.5194/acp-11-11267-2011>
- Clem KR, Fogt RL (2015) South Pacific circulation changes and their connection to the tropics and regional Antarctic warming in austral spring, 1979–2012. *J Geophys Res Atmos* 120:2773–2792. <https://doi.org/10.1002/2014JD022940>
- Clem KR, Renwick JA, McGregor J, Fogt RL (2016) The relative influence of ENSO and SAM on Antarctic Peninsula climate. *J Geophys Res Atmos* 121:9324–9341. <https://doi.org/10.1002/2016JD025305>
- Conolley WM (1997) Variability in annual mean circulation in southern high latitudes. *Clim Dyn* 13:745–756
- Deser C, Phillips AS, Alexander MA (2010) Twentieth century tropical sea surface temperature trends revisited. *Geophys Res Lett*. <https://doi.org/10.1029/2010GL043321>
- Ding Q, Steig EJ (2013) Temperature change on the Antarctic Peninsula linked to the tropical Pacific. *J Clim* 26:7570–7585
- Ding Q, Steig EJ, Battisti DS, Küttel M (2011) Winter warming in West Antarctica caused by central tropical Pacific warming. *Nat Geosci* 4:398–403. <https://doi.org/10.1038/ngeo1129>
- England MR, Polvani LM, Smith KL et al (2016) Robust response of the Amundsen Sea Low to stratospheric ozone depletion. *Geophys Res Lett* 43:8207–8213. <https://doi.org/10.1002/2016GL070055>
- Eyring V, Arblaster JM, Cionni I et al (2013) Long-term ozone changes and associated climate impacts in CMIP5 simulations. *J Geophys Res Atmos* 118:5029–5060. <https://doi.org/10.1002/jgrd.50316>
- Fogt RL, Wovrosh AJ (2015) The relative influence of tropical sea surface temperatures and radiative forcing on the Amundsen Sea Low. *J Clim* 28:8540–8555. <https://doi.org/10.1175/JCLI-D-15-0091.1>
- Fogt RL, Zbacnik EA (2014) Sensitivity of the Amundsen Sea Low to Stratospheric Ozone Depletion. *J Clim* 27:9383–9400. <https://doi.org/10.1175/JCLI-D-13-00657.1>
- Fogt RL, Perlwitz J, Monaghan AJ et al (2009) Historical SAM variability. Part II: twentieth-century variability and trends from reconstructions, observations, and the IPCC AR4 models. *J Clim* 22:5346–5365. <https://doi.org/10.1175/2009JCLI2786.1>
- Fogt RL, Bromwich DH, Hines KM (2011) Understanding the SAM influence on the South Pacific ENSO teleconnection. *Clim Dyn* 36:1555–1576. <https://doi.org/10.1007/s00382-010-0905-0>
- Fogt RL, Goergens CA, Jones ME et al (2016a) Antarctic station-based seasonal pressure reconstructions since 1905: 1. Reconstruction evaluation. *J Geophys Res Atmos* 121:2814–2835. <https://doi.org/10.1002/2015JD024564>
- Fogt RL, Jones JM, Goergens CA et al (2016b) Antarctic station-based seasonal pressure reconstructions since 1905: 2. Variability and trends during the twentieth century. *J Geophys Res Atmos* 121:2836–2856. <https://doi.org/10.1002/2015JD024565>
- Fogt RL, Goergens CA, Jones JM et al (2017a) A twentieth century perspective on summer Antarctic pressure change and variability and contributions from tropical SSTs and ozone depletion. *Geophys Res Lett* 44:9918–9927. <https://doi.org/10.1002/2017GL075079>

- Fogt RL, Jones ME, Solomon S et al (2017b) An exceptional summer during the south pole race of 1911–1912. *Bull Am Meteorol Soc.* <https://doi.org/10.1175/BAMS-D-17-0013.1>
- Henley BJ, Gergis J, Karoly DJ et al (2015) A tripole index for the interdecadal Pacific oscillation. *Clim Dyn* 45:3077–3090. <https://doi.org/10.1007/s00382-015-2525-1>
- Huang B, Banzon VF, Freeman E et al (2015) Extended reconstructed sea surface temperature version 4 (ERSST.v4). Part I: upgrades and intercomparisons. *J Clim* 28:911–930. <https://doi.org/10.1175/JCLI-D-14-00006.1>
- Huang B, Thorne PW, Banzon VF et al (2017) Extended reconstructed sea surface temperature, version 5 (ERSSTv5): upgrades, validations, and intercomparisons. *J Clim* 30:8179–8205. <https://doi.org/10.1175/JCLI-D-16-0836.1>
- Jones JM, Gille ST, Goosse H et al (2016) Assessing recent trends in high-latitude Southern Hemisphere surface climate. *Nat Clim Change* 6:917–926. <https://doi.org/10.1038/nclimate3103>
- Marshall GJ (2003) Trends in the southern annular mode from observations and reanalyses. *J Clim* 16:4134–4143. [https://doi.org/10.1175/1520-0442\(2003\)016%3C4134:TITSA%3E2.0.CO;2](https://doi.org/10.1175/1520-0442(2003)016%3C4134:TITSA%3E2.0.CO;2)
- Meehl GA, Arblaster JM, Bitz CM et al (2016) Antarctic sea-ice expansion between 2000 and 2014 driven by tropical Pacific decadal climate variability. *Nat Geosci* 9:590–595. <https://doi.org/10.1038/ngeo2751>
- Miller RL, Schmidt GA, Shindell DT (2006) Forced annular variations in the 20th century Intergovernmental Panel on Climate Change Fourth Assessment Report models. *J Geophys Res.* <https://doi.org/10.1029/2005JD006323>
- Monaghan AJ, Bromwich DH, Chapman W, Comiso JC (2008) Recent variability and trends of Antarctic near-surface temperature. *J Geophys Res.* <https://doi.org/10.1029/2007JD009094>
- Neale RB, Chen C-C, Gettelman A et al (2010) Description of the NCAR community atmosphere model (CAM5.0). NCAR, Boulder
- Nicolas JP, Bromwich DH (2014) New reconstruction of antarctic near-surface temperatures: multidecadal trends and reliability of global reanalyses. *J Clim* 27:8070–8093. <https://doi.org/10.1175/JCLI-D-13-00733.1>
- O'Donnell R, Lewis N, McIntyre S, Condon J (2011) Improved methods for PCA-based reconstructions: case study using the Steig et al. (2009) Antarctic temperature reconstruction. *J Clim* 24:2099–2115. <https://doi.org/10.1175/2010JCLI3656.1>
- Polvani LM, Waugh DW, Correa GJP, Son S-W (2011) Stratospheric ozone depletion: the main driver of twentieth-century atmospheric circulation changes in the Southern Hemisphere. *J Clim* 24:795–812. <https://doi.org/10.1175/2010JCLI3772.1>
- Purich A, England MH, Cai W et al (2016) Tropical Pacific SST drivers of recent Antarctic sea ice trends. *J Clim* 29:8931–8948. <https://doi.org/10.1175/JCLI-D-16-0440.1>
- Raphael MN, Marshall GJ, Turner J et al (2016) The Amundsen Sea Low: variability, change, and impact on Antarctic climate. *Bull Am Meteorol Soc* 97:111–121. <https://doi.org/10.1175/BAMS-D-14-00018.1>
- Schneider DP, Fogt RL (2018) Artifacts in century-length atmospheric and coupled reanalyses over Antarctica due to historical data availability. *Geophys Res Lett.* <https://doi.org/10.1002/2017GL076226>
- Schneider DP, Deser C, Okumura Y (2012) An assessment and interpretation of the observed warming of West Antarctica in the austral spring. *Clim Dyn* 38:323–347. <https://doi.org/10.1007/s00382-010-0985-x>
- Schneider DP, Deser C, Fan T (2015) Comparing the impacts of tropical SST variability and polar stratospheric ozone loss on the Southern Ocean westerly winds. *J Clim* 28:9350–9372. <https://doi.org/10.1175/JCLI-D-15-0090.1>
- Smith TM, Reynolds RW, Peterson TC, Lawrimore J (2008) Improvements to NOAA's historical merged land–ocean surface temperature analysis (1880–2006). *J Clim* 21:2283–2296. <https://doi.org/10.1175/2007JCLI2100.1>
- Solomon A, Newman M (2012) Reconciling disparate twentieth-century Indo-Pacific ocean temperature trends in the instrumental record. *Nat Clim Change* 2:691–699. <https://doi.org/10.1038/nclimate1591>
- Stammerjohn SE, Martinson DG, Smith RC et al (2008) Trends in Antarctic annual sea ice retreat and advance and their relation to El Niño–Southern Oscillation and Southern Annular Mode variability. *J Geophys Res.* <https://doi.org/10.1029/2007JC004269>
- Staten PW, Rutz JJ, Reichler T, Lu J (2012) Breaking down the tropospheric circulation response by forcing. *Clim Dyn* 39:2361–2375. <https://doi.org/10.1007/s00382-011-1267-y>
- Steig EJ, Schneider DP, Rutherford SD et al (2009) Warming of the Antarctic ice-sheet surface since the 1957 International Geophysical Year. *Nature* 457:459–462. <https://doi.org/10.1038/nature07669>
- Thompson DWJ, Solomon S (2002) Interpretation of recent Southern Hemisphere climate change. *Science* 296:895–899. <https://doi.org/10.1126/science.1069270>
- Turner J (2004) The El Niño–Southern Oscillation and Antarctica. *Int J Climatol* 24:1–31. <https://doi.org/10.1002/joc.965>
- Turner J, Colwell SR, Marshall GJ, et al (2004) The SCAR READER project: toward a high-quality database of mean Antarctic meteorological observations. *J Clim* 17:2890–2898. [https://doi.org/10.1175/1520-0442\(2004\)017%3C2890:TSRPTA%3E2.0.CO;2](https://doi.org/10.1175/1520-0442(2004)017%3C2890:TSRPTA%3E2.0.CO;2)
- Turner J, Colwell SR, Marshall GJ et al (2005) Antarctic climate change during the last 50 years. *Int J Climatol* 25:279–294. <https://doi.org/10.1002/joc.1130>
- Turner J, Lu H, White I et al (2016) Absence of 21st century warming on Antarctic Peninsula consistent with natural variability. *Nature* 535:411–415. <https://doi.org/10.1038/nature18645>
- Wilson AB, Bromwich DH, Hines KM (2016) Simulating the mutual forcing of anomalous high southern latitude atmospheric circulation by El Niño flavors and the Southern Annular Mode. *J Clim* 29:2291–2309. <https://doi.org/10.1175/JCLI-D-15-0361.1>
- Zazulie N, Rusticucci M, Solomon S (2010) Changes in climate at high southern latitudes: a unique daily record at Orcadas spanning 1903–2008. *J Clim* 23:189–196. <https://doi.org/10.1175/2009JCLI3074.1>

Publisher's Note Springer Nature remains neutral with regard to jurisdictional claims in published maps and institutional affiliations.